



Modulation of the QBO on the MJO-related surface air temperature anomalies over Eurasia during boreal winter

Lei Song¹ · Renguang Wu^{1,2}

Received: 21 August 2019 / Accepted: 7 January 2020 / Published online: 13 January 2020
© Springer-Verlag GmbH Germany, part of Springer Nature 2020

Abstract

Previous studies have indicated the modulation of the Madden–Julian oscillation (MJO) by the Quasi-Biennial Oscillation (QBO) and the influence of the MJO on surface temperature over Eurasia during boreal winter. The present study reveals that the MJO-related circulation anomalies are different in easterly and westerly QBO years, leading to distinct surface temperature anomaly patterns over Eurasia. During the easterly QBO years, the surface air temperature anomalies over Eurasia display a meridional dipole pattern in MJO phase 2 associated with the mid-latitude surface anticyclonic anomalies. The development of surface anomalous anticyclone is attributed to a combined effect of negative North Atlantic Oscillation (NAO)-related mid-latitude wave train and stronger MJO convection triggered poleward propagation of Rossby wave train. The negative NAO is related to the easterly QBO through the Holton–Tan relationship. The anomalous overturning circulation excited by the stronger MJO convection in easterly QBO years also contributes to the development and eastward extension of anomalous anticyclone. The anticyclonic anomalies induce the meridional temperature anomaly pattern by horizontal advection. During the westerly QBO years, the surface air temperature anomalies over Eurasia show a zonal alternating pattern in MJO phase 3, which corresponds to the development of mid-latitude Rossby wave train associated with positive NAO with a stronger MJO–NAO connection in westerly QBO years. The MJO convection induces upper-level divergent wind anomalies, contributing partially to the development of the Rossby wave source and helping the building of the mid-latitude wave train. The zonal temperature anomalies over Eurasia are also contributed by the horizontal advection associated with surface cyclonic anomalies.

Keywords MJO · Eurasian temperature anomaly pattern · QBO phases · Mid-latitude wave train · Poleward wave propagation

1 Introduction

The Madden–Julian oscillation (MJO) is the dominant intra-seasonal variability in the tropics (Madden and Julian 1971, 1972). It manifests as eastward propagation of precipitation and convection systems from the tropical Indian Ocean to the central Pacific with a time period of 30–90 days (Zhang 2005). The MJO can influence mid- to high-latitude weather and climate via exciting poleward dispersion of Rossby wave

energy by upper-tropospheric divergence (Sardeshmukh and Hoskins 1988; Seo and Lee 2017). Previous studies have found the connection between the MJO and surface air temperature variation over East Asia (Jeong et al. 2005; He et al. 2011; Seo et al. 2017; Abdillah et al. 2018). Song and Wu (2019a) indicated that the impacts of the MJO on cold anomalies over eastern China depend on the phase of the Arctic Oscillation (AO). Song and Wu (2019b) showed that the MJO and AO connection differs in early and late winter, which leads to a different relationship between the MJO and surface air temperature over East Asia during early and late winter. The variation of mean state from early to late winter can be linked to the change in the relationship between the tropical Atlantic Ocean sea surface temperature and the stratospheric polar vortex (Rao and Ren 2018). The MJO convection can also trigger anomalous meridional overturning circulation by which the mid-latitude Siberian high is

✉ Renguang Wu
renguang@zju.edu.cn

¹ Center for Monsoon System Research, Institute of Atmospheric Physics, Chinese Academy of Sciences, Beijing, China

² School of Earth Sciences, Zhejiang University, Hangzhou, China

intensified, leading to cold anomalies over East Asia (Song and Wu 2019c). The MJO can also be connected to the North Atlantic Oscillation (NAO) with the relationship similar to that between the MJO and the AO. The MJO convection over the tropical Indian Ocean is followed by the positive NAO, and the MJO convection over the western Pacific is followed by the negative NAO (Cassou 2008; Lin et al. 2009; Rao and Ren 2016).

The Quasi-Biennial Oscillation (QBO) in the stratosphere is characterized as alternation of easterly and westerly zonal winds over the tropics with a period of about 28 months (Baldwin et al. 2001; Nishimoto and Yoden 2017; Andrews et al. 2019). The QBO can be linked to the stratospheric polar vortex by the modification of the propagation of the stationary planetary waves (Rao and Ren 2017, 2018; Rao et al. 2019; Andrews et al. 2019). Furthermore, the stratospheric polar vortex is closely linked to the AO, which results in a possible connection between the QBO and AO (Andrews et al. 2019). The variation of the stratospheric polar vortex can impact surface weather and climate (Baldwin and Dunkerton 2001; Gray et al. 2018). As such, there may be an influence of the QBO on extratropical tropospheric climate. By inducing meridional circulation, the QBO can modify the tropospheric subtropical jet and the activity of tropospheric Rossby waves through which the QBO affects surface climate (Garfinkel and Hartmann 2011; Gray et al. 2018).

The MJO is modulated by the QBO during boreal winter. Studies indicated that the QBO explains about 40% of inter-annual variation of the MJO during boreal winter (Son et al. 2017; Peña-Ortiz et al. 2019). During easterly wind QBO phase (EQBO), the MJO tends to be manifested as slower eastward propagation of convection, leading to more prolonged MJO events, and the MJO convection can propagate much further eastward during EQBO than westerly wind QBO phase (WQBO), which is accompanied by stronger MJO during EQBO than WQBO phases (Yoo and Son 2016; Son et al. 2017; Nishimoto and Yoden 2017; Hendon and Abhik 2018; Zhang and Zhang 2018; Andrews et al. 2019). The MJO–QBO connection may be related to the variation in the static stability at the tropopause caused by the QBO, which can influence the development of deep convection associated with the MJO (Yoo and Son 2016; Son et al. 2017; Nishimoto and Yoden 2017; Hendon and Abhik 2018). The MJO–NAO connection can be modulated by the QBO. During the WQBO phase, the MJO–NAO connection is stronger, which is related to the stronger subtropical jet stream over the North Pacific, providing more favorable condition for the meridional propagation of the Rossby wave train emanating from the tropics that connects the MJO and the NAO (Feng and Lin 2019).

Previous studies have suggested the modulation of the QBO on the MJO features in the tropics (Liu et al. 2014;

Yoo and Son 2016; Zhang and Zhang 2018). Whether the impacts of the MJO on mid- to high-latitude weather and climate over Eurasia are modulated by the QBO is worthy of investigation. Since the mid-latitude atmospheric circulations associated with the MJO are quite different in EQBO and WQBO (Son et al. 2017), it raises the possibility that the MJO-related intraseasonal surface air temperature anomalies over Eurasia may depend on the QBO phase. In this study, we address this issue by comparing intraseasonal surface air temperature anomalies over Eurasia associated with the MJO in EQBO and WQBO years during boreal winter. In addition, we investigate the differences of the processes connecting the MJO and mid- to high-latitude temperature variations between EQBO and WQBO years.

In the following, the dataset and methodology are described in Sect. 2. Different features of the MJO related anomalies over Eurasia in EQBO and WQBO years are illustrated in Sect. 3. In Sect. 4, atmospheric processes contributing to the different features are analyzed. A brief summary and some discussions are given in Sect. 5.

2 Data and methodology

In this study, we use the daily output from the National Centers for Environmental Prediction (NCEP)–Department of Energy (DOE) Reanalysis 2 provided by the National Oceanic and Atmospheric Administration (NOAA)/Office of Oceanic and Atmospheric Research/Earth System Research Laboratory Physical Science Division (Kanamitsu et al., 2002). We focus on boreal winters (December, January, and February) from 1979 to 2016. The daily variables we used in this study include surface air temperature, surface wind, sea level pressure, geopotential height, air temperature, meridional and zonal winds at different levels. The surface air temperature and wind are on the T62 Gaussian grid. The pressure level variables are available on a horizontal resolution of $2.5^\circ \times 2.5^\circ$ with 17 vertical layers extending from 1000 to 10 hPa.

The MJO phases are identified using daily Real-time Multivariate MJO (RMM) index (Wheeler and Hendon 2004), which is obtained from the website of the Bureau of Meteorology of Australia (<http://www.bom.gov.au/climate/mjo/graphics/rmm.74toRealttime.txt>). The amplitude of the MJO is defined as $\sqrt{RMM1^2 + RMM2^2}$.

The QBO index in this study is defined following Nishimoto and Yoden (2017), which is monthly mean zonal-mean zonal wind at 50 hPa from 10° S to 10° N (U50). One-half of the standard deviation of the QBO index is selected as the threshold to determine the EQBO and WQBO. If the U50 is less than or equal to one-half of the standard deviation below the time mean (-7.64 m/s), the EQBO is defined. If the U50 is larger than or equal to

one-half of the standard deviation above the time mean (2.17 m/s), the WQBO is defined. In order to exclude the influence of El Niño-Southern Oscillation (ENSO), only neutral ENSO winters are considered in selecting the EQBO and WQBO years. Neutral ENSO winters are those when the oceanic Niño Index (ONI) falls between ± 1 °C. The ONI index can be found on the National Weather Service, Climate Prediction Center website (https://origin.cpc.ncep.noaa.gov/products/analysis_monitoring/ensos_tuff/ONI_v5.php). We identified 8 EQBO winters and 10 WQBO winters in total 37 winters (Table 1). The daily NAO index is obtained from <https://www.cpc.ncep.noaa.gov/products/precip/CWlink/pna/nao.shtml>.

Based on the MJO phases, composite analysis is performed on the 5-day average after each MJO phase, following Li et al. (2018) and Song and Wu (2019a), during which the amplitude of the MJO exceeds one standard deviation. The significance of the composite quantities is estimated based on the Student’s *t* test. All the variables are filtered using the Butterworth filter to extract the 30–60 day intraseasonal signal. The propagation of the tropospheric Rossby wave packets is illustrated by the Rossby wave activity flux (Takaya and Nakamura 2001).

The Rossby wave source associated with the Rossby wave train is investigated following the linearized barotropic vorticity equation (Sardeshmukh and Hoskins 1988; Seo and Lee 2017; Tseng et al. 2019):

$$\frac{\partial \zeta'}{\partial t} = S' - \overline{\vec{V}}_{\psi} \cdot \nabla \zeta' - \overline{\vec{V}}'_{\psi} \cdot \nabla \bar{\zeta} + F.$$

In the above equation, the prime denotes the intraseasonal parts (30–60 day), the overbar represents the means of all the EQBO or WQBO years, respectively, ζ is the absolute vorticity, $\overline{\vec{V}}_{\psi}$ is the rotational wind, S is the Rossby wave source (RWS), and F is the frictional term. The RWS is related to terms associated with the divergent winds:

$$S' = -\bar{\zeta} \nabla \cdot \overline{\vec{V}}'_{\chi} - \overline{\vec{V}}'_{\chi} \cdot \nabla \bar{\zeta} - \zeta' \nabla \cdot \overline{\vec{V}}_{\chi} - \overline{\vec{V}}_{\chi} \cdot \nabla \zeta'.$$

In the above equation, $\overline{\vec{V}}_{\chi}$ denotes divergent winds. The first term on the right side represents stretching of mean absolute vorticity by divergence of the anomalous divergent wind, the second term denotes the advection of mean absolute vorticity by the anomalous divergent wind,

and the third and fourth terms are stretching of anomalous vorticity by the mean divergent wind and advection of anomalous vorticity by mean divergent wind, respectively (Tseng et al. 2019).

To investigate the intraseasonal variations of surface air temperature, the thermodynamic equation is employed to evaluate contributions from different components. The thermodynamic equation can be written as (Holton 2004; Hegyi and Deng 2017):

$$\frac{\partial T'}{\partial t} = -(\overline{\vec{V}} \cdot \nabla T)' + \left[\omega \left(\kappa \frac{T}{p} - \frac{\partial T}{\partial p} \right) \right]' + Q'.$$

In the above equation, the prime denotes the intraseasonal parts (30–60 day), T is surface air temperature, $\overline{\vec{V}}$ is surface winds, p is pressure, ω is vertical p-velocity, $\kappa = R_d/c_p$, R_d is the gas constant for dry air, c_p is the specific heat capacity of air, and Q is the net heat flux. On the right-hand side of the equation, the first term represents horizontal advection, the second term denotes adiabatic heating related to vertical motion, and the third term is diabatic heating. In this study, the diabatic heating is obtained as the residue of the budget on the right-hand side of the equation. The horizontal advection can be divided into four terms:

$$\overline{\vec{V}} \cdot \nabla T' \sim \bar{u} \frac{\partial T'}{\partial x} + u' \frac{\partial \bar{T}}{\partial x} + \bar{v} \frac{\partial T'}{\partial y} + v' \frac{\partial \bar{T}}{\partial y} + \bar{v}' \frac{\partial T'}{\partial y} + u' \frac{\partial T'}{\partial x}.$$

In this study, we only consider the terms associated with the means of all the EQBO and WQBO years, and the second order terms are dropped.

3 Different MJO-related anomalies in EQBO and WQBO years

Previous studies have indicated that the MJO convection over the tropical Indian Ocean (i.e., MJO phases 2–3) can lead to evident surface air temperature anomalies over Eurasia (Jeong et al. 2005; He et al. 2011; Song and Wu 2019a, c). Cold anomalies tend to appear over Central and East Asia and warm anomalies over high latitudes of Eurasia accompanying MJO phases 2–3 (see Fig. 1b, c of Song and Wu 2019a). A question is if the above temperature anomaly pattern remains when the EQBO and WQBO years are considered separately. Furthermore, after comparing the surface temperature anomalies in all the eight MJO phases during both EQBO and WQBO years,

Table 1 The EQBO and WQBO years in neutral ENSO years

	Years
EQBO	1979/1980; 1989/1990; 1996/1997; 2001/2002; 2003/2004; 2005/2006; 2012/2013; 2014/2015
WQBO	1980/1981; 1985/1986; 1987/1988; 1990/1991; 1995/1996; 2002/2003; 2004/2005; 2006/2007; 2008/2009; 2013/2014

the difference of anomalous surface temperature signal over the Eurasian continent between EQBO and WQBO years are more evident in MJO phases 2 and 3. In the following, we compare composite 30–60 day surface air temperature anomalies in MJO phases 2–3 constructed based on the EQBO and WQBO years.

In MJO phase 2, surface air temperature anomalies display a meridional dipole pattern over Eurasia in both EQBO and WQBO years (Fig. 1a, b). Warm anomalies are located north of 60° N and cold anomalies extend from Central to East Asia. This dipole pattern resembles that in Fig. 1b of Song and Wu (2019a) expect for a stronger warm signal in the high latitudes. In MJO phase 3, temperature anomaly distribution is very different between EQBO and WQBO years. In EQBO years, the warm anomalies in the high latitudes move eastward and are weakened and the cold anomalies move southeastward and are also weakened (Fig. 1c). In WQBO years, surface air temperature anomalies switch to a northwest-southeast contrast pattern (Fig. 1d). Cold

anomalies are situated over eastern Europe and warm anomalies are lying over Central Asia. Another cold anomaly region extends from the Lake Baikal to northeast China. The different temperature anomaly patterns in EQBO and WQBO years suggest a modulation of the QBO on the impact of the MJO upon climate over Eurasia.

The development of surface air temperature anomalies is closely linked to warm or cold air advection by surface wind anomalies (Song and Wu 2017). In MJO phase 2, surface anticyclonic wind anomalies extend zonally from Europe to Siberia with two centers situating over Europe and the Lake Baikal in EQBO years (Fig. 2a). Anomalous cyclone covers Asia south of 40° N. The southerly wind anomalies on the northwestern and northern flanks of the anomalous anticyclone account for the warm anomalies over the high latitudes and the northerly wind anomalies on the southern flank of the anomalous anticyclone contribute to the cold anomalies in the mid-latitudes (Fig. 1a). The distribution of surface pressure and wind anomalies in WQBO years (Fig. 2b) is

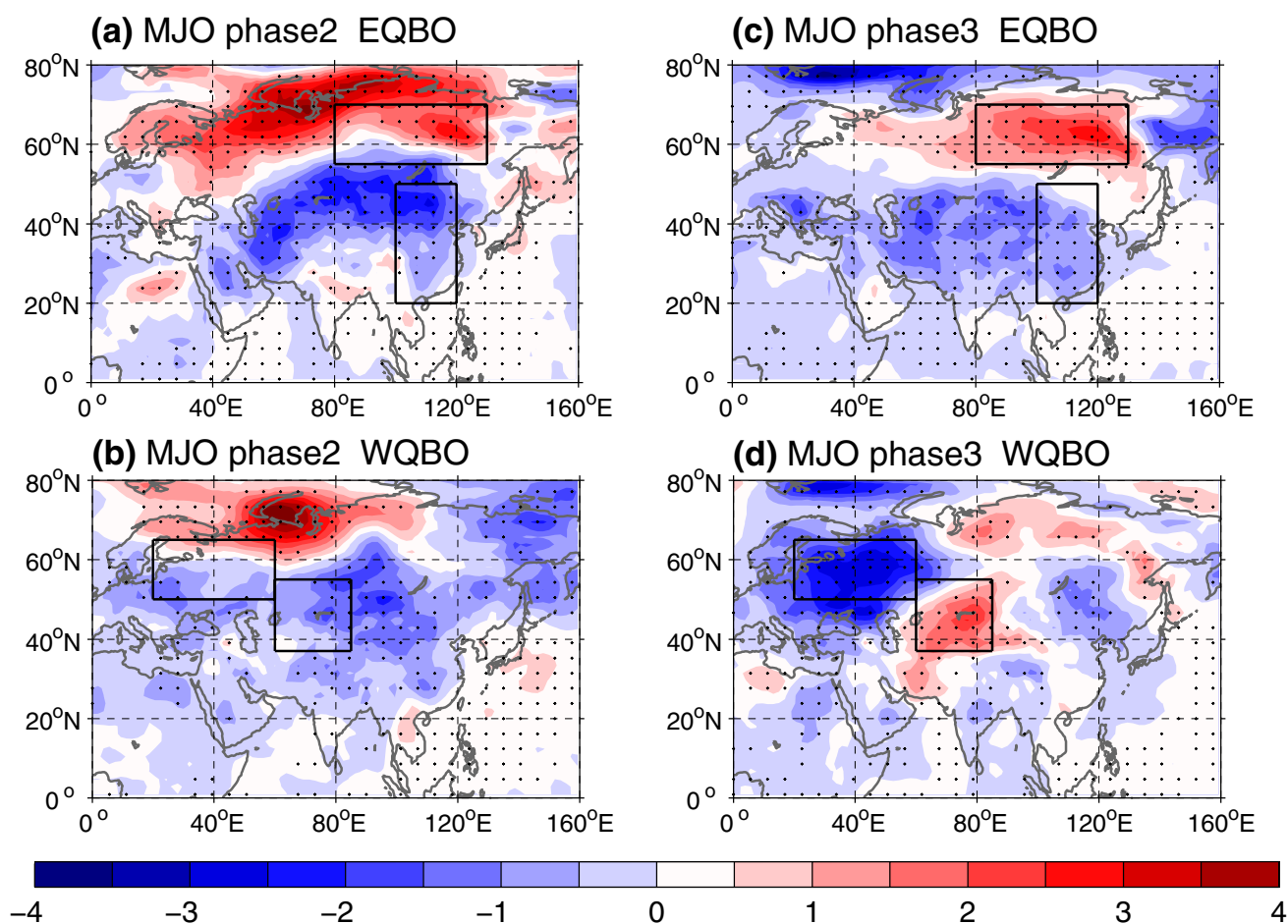


Fig. 1 Composite surface air temperature anomalies (shading, °C) in MJO phases 2 (**a**, **b**) and 3 (**c**, **d**) in EQBO (**a**, **c**) and WQBO (**b**, **d**) years. Black dots denote temperature anomalies significant at the 95%

confidence level. Black boxes indicate the regions where area-mean are calculated in Fig. 3

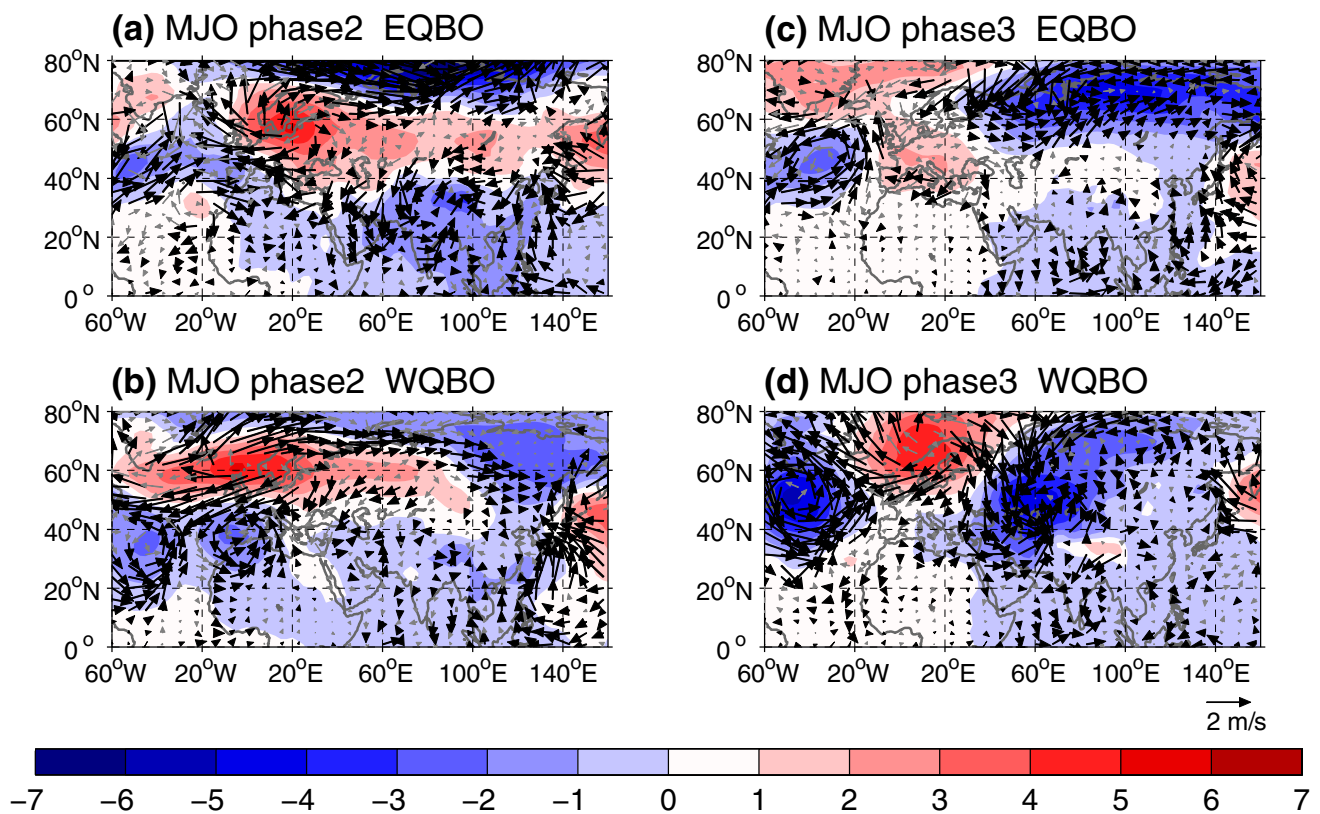


Fig. 2 Composite sea level pressure anomalies (shading, hPa) and surface wind anomalies (vector, scale on right bottom) in MJO phases 2 (a, b) to 3 (c, d) in EQBO (a, c) and WQBO (b, d) years. Black vectors denote wind anomalies significant at the 95% confidence level

similar to that in EQBO years (Fig. 2a). However, the anomalous anticyclone is weaker and is situated more westward. Correspondingly, cold anomalies in the mid-latitudes extend more westward (Fig. 1b).

In MJO phase 3, anomalous cyclone dominates the region north of 60° N of Eurasia, accompanied by southerly wind anomalies around 60° N in EQBO years (Fig. 2c), which explains the warm anomalies in high-latitude Russia (Fig. 1c). The anticyclonic anomalies over Eurasia are weakened (Fig. 2c), corresponding to weak anomalies there (Fig. 1c). In WQBO years, strong anomalous surface cyclone appears over Central Asia (Fig. 2d). The northerly wind anomalies on its western flank and southerly wind anomalies on its eastern flank contribute to cold anomalies over eastern Europe and warm anomalies over Central Asia, respectively (Fig. 1d). There is an anomalous anticyclone over the northwest coast of Europe (Fig. 2d).

Different terms of thermodynamic energy equation are evaluated to illustrate the processes associated with the intra-seasonal temperature variations over Eurasia during MJO phases 2–3 in both EQBO and WQBO years. We select a couple of regions to demonstrate the specific processes important to the temperature anomalies. In EQBO years, we focus on warm anomalies over northern Siberia (55°–70° N,

80°–130° E) and cold anomalies over East Asia (20°–50° N, 100°–120° E) in MJO phase 2. In WQBO years, we examine cold anomalies over eastern Europe (50°–65° N, 20°–60° E) and warm anomalies over western Siberia (37°–55° N, 60°–85° E) in MJO phase 3.

During MJO phase 2 in EQBO years, the warm anomalies over northern Siberia are mainly contributed by the horizontal advection and the diabatic heating is small (Fig. 3a). The adiabatic heating has a damping effect. The positive horizontal advection is contributed by the advection of mean temperature by anomalous winds ($-u' \frac{\partial \bar{T}}{\partial x}$ and $-v' \frac{\partial \bar{T}}{\partial y}$) (Fig. 3e), which is related to the development of surface anticyclonic anomalies (Fig. 2a). Likewise, the cold anomalies over East Asia are mainly contributed by the horizontal advection and adiabatic heating is secondary (Fig. 3b). Diabatic heating damps the cooling in this case. The cooling effect of the horizontal advection is contributed by the advection of mean temperature by anomalous meridional wind ($-v' \frac{\partial \bar{T}}{\partial y}$) and anomalous temperature advection by mean zonal wind ($-\bar{u} \frac{\partial T'}{\partial x}$) (Fig. 3f).

During MJO phase 3 in WQBO years, the cold anomalies over eastern Europe is contributed by the horizontal advection and diabatic heating (Fig. 3c). The adiabatic

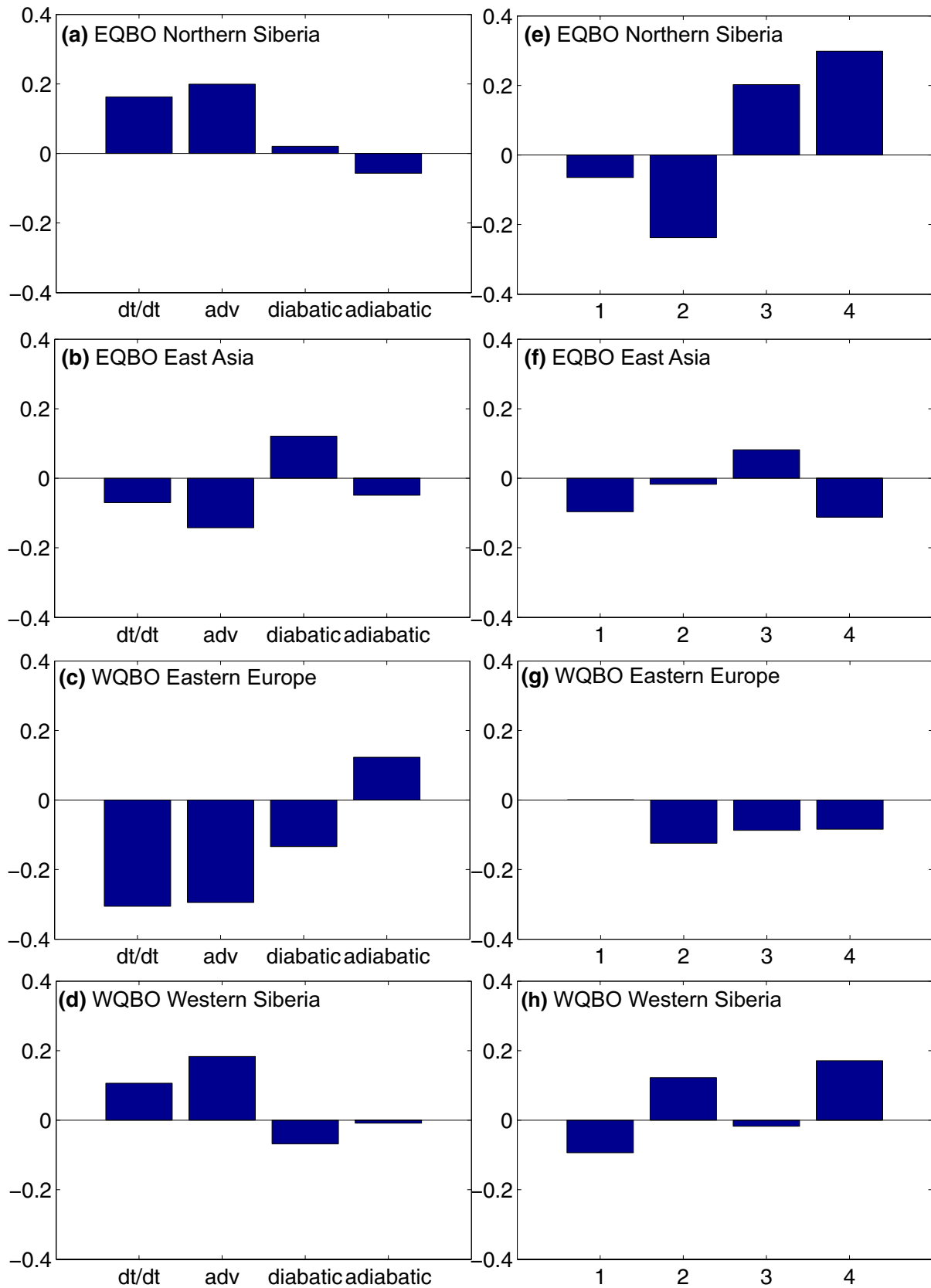


Fig. 3 Different terms in the thermodynamic equation (**a–d**) and different parts related to advection term (**e–h**) averaged over the regions of (**a, e**) northern Siberia (55° N– 70° N, 80° E– 130° E) in EQBO years, **b, f** East Asia (20° N– 50° N, 100° E– 120° E) in EQBO years, **c, g** eastern Europe (50° N– 65° N, 20° E– 60° E) in WQBO years and **d, h** western Siberia (37° N– 55° N, 60° E– 85° E) in WQBO years. The labels from 1 to 4 in **e–h** indicate $-\bar{u}'\frac{\partial T'}{\partial x}$, $-\bar{v}'\frac{\partial T'}{\partial y}$, $-u'\frac{\partial T'}{\partial x}$, $-v'\frac{\partial T'}{\partial y}$

heating has a damping effect. The horizontal advection is contributed by the advection of mean temperature by anomalous winds ($-u'\frac{\partial T'}{\partial x}$ and $-v'\frac{\partial T'}{\partial y}$) and anomalous temperature advection by mean meridional wind ($-\bar{v}'\frac{\partial T'}{\partial y}$) (Fig. 3g). The warm anomalies over western Siberia are controlled by the horizontal advection and damped by the diabatic heating (Fig. 3d). The anomalous warm advection is contributed by the advection of mean temperature by anomalous meridional wind ($-v'\frac{\partial T'}{\partial y}$) and anomalous temperature advection by mean meridional wind ($-\bar{v}'\frac{\partial T'}{\partial y}$) (Fig. 3h). The development of the advection of mean temperature by anomalous winds is related to surface cyclonic anomalies over Central Asia (Fig. 2d).

The development of surface cyclonic and anticyclonic anomalies is linked to the upper-tropospheric Rossby wave pattern (Song et al. 2016). In MJO phase 2, a mid-latitude

wave train is observed over Eurasia, as indicated by the Rossby wave activity fluxes (Fig. 4a). The anomalous high at upper-troposphere over eastern Europe corresponds to surface anomalous anticyclone (Fig. 2a), indicative of a quasi-barotropic vertical structure. The anomalous low over Central and East Asia explains the development of anomalous surface anticyclone that contributes to cold anomalies in situ (Figs. 1a, 2a, 4a) (Song and Wu 2017). Another branch of Rossby wave activity fluxes originates from the anomalous high over India and extends to East Asia (Fig. 4a), which is a response to the MJO convection over the tropical Indian Ocean (Jin and Hoskins 1995; Song and Wu 2019a). It also contributes to the development of anomalous low over East Asia (Fig. 4a). The wave pattern in MJO phase 2 of WQBO years is weak (Fig. 4b), so is in MJO phase 3 of EQBO years (Fig. 4c).

In MJO phase 3 of WQBO years, a mid-latitude wave train is observed over Eurasia (Fig. 4d). It extends more zonally compared to that in MJO phase 2 of EQBO years. This corresponds to the zonal distribution of surface temperature and pressure anomalies (Figs. 1d, 2d). The anomalous high associated with the MJO convection locates more westward compared to EQBO years (Fig. 4c). A poleward Rossby wave propagation is seen from South Asia to East Asia.

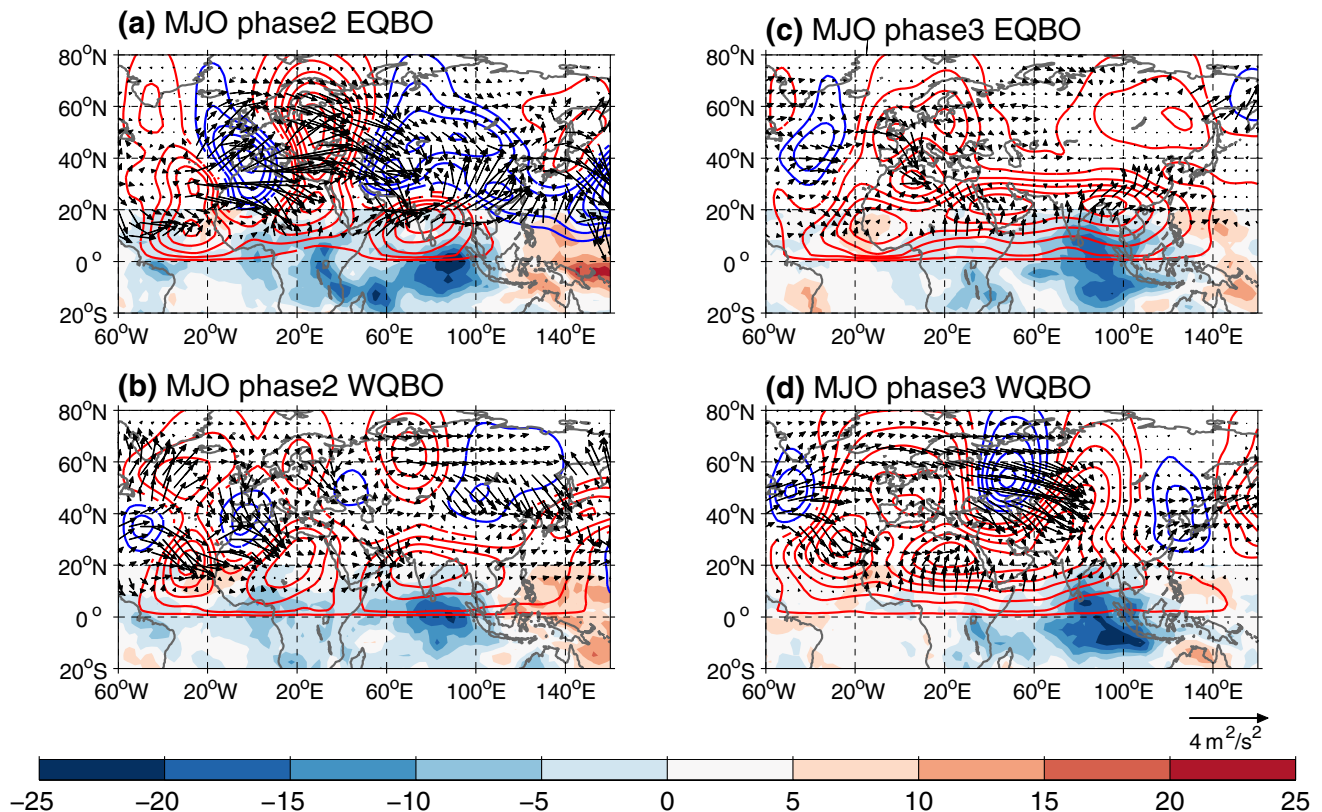


Fig. 4 Composite outgoing longwave radiation (OLR) anomalies (shading, W/m^2) between 20° S and 20° N, stream function anomalies (contour, blue and red contours indicate negative and positive anomalies, respectively, $\times 10^6 \text{ m}^2/\text{s}^2$), and wave activity fluxes (m^2/s^2) (vector, scale at the right-bottom) at 300 hPa in MJO phases 2 (**a, b**) to 3 (**c, d**) in EQBO (**a, c**) and WQBO (**b, d**) years

lies, respectively, $\times 10^6 \text{ m}^2/\text{s}^2$), and wave activity fluxes (m^2/s^2) (vector, scale at the right-bottom) at 300 hPa in MJO phases 2 (**a, b**) to 3 (**c, d**) in EQBO (**a, c**) and WQBO (**b, d**) years

Comparing EQBO and WQBO years, the poleward Rossby wave train triggered by the MJO convection is stronger in phase 2 of EQBO years. This feature agrees with the result of previous studies that the MJO is stronger during EQBO than WQBO (Yoo and Son 2016; Son et al. 2017; Nishimoto and Yoden 2017; Hendon and Abhik 2018; Zhang and Zhang 2018; Andrews et al. 2019), which leads to stronger poleward Rossby wave train over the North Pacific.

The sea level pressure map shows positive anomalies over southern Greenland and negative anomalies over mid-latitude North Atlantic in MJO phase 2 of the EQBO years (Fig. 2a), which corresponds to negative NAO phase in Fig. 5a, contributing to the building of Rossby wave train over the Eurasian continent (Watanabe 2004) and the development of surface air temperature anomalies over Eurasia in EQBO years (Fig. 1a). We can infer from Fig. 5a that the NAO tends to be negative in EQBO years, which can be explained by the Holton–Tan relationship (Holton and Tan 1980, 1982; Rao et al. 2019). In EQBO years, the zero wind line at 50-hPa moves to subtropics, which leads to the confinement of upward propagation of tropospheric planetary waves in the extratropics. The poleward planetary wave propagation is more evident, contributing to the weakening of the polar vortex (Andrews et al. 2019) and negative NAO through downward propagation of stratospheric signals (Baldwin and Dunkerton 2001).

In WQBO years, the NAO is positive in MJO phase 3 (Fig. 5b), which is consistent with negative sea level pressure anomalies over southern Greenland (Fig. 2d), and it leads to the mid-latitude wave train (Fig. 4d) that contributes to the zonal pattern of temperature anomalies over Eurasia (Fig. 1d). The NAO is positive in MJO phases 3, and negative in MJO phase 7, which confirms that the MJO-NAO connection is stronger in WQBO years (Feng and Lin 2019).

4 Interpretation of MJO-related atmospheric circulation anomalies in EQBO and WQBO years

To understand the difference of the MJO-related atmospheric circulation anomalies over Eurasia between EQBO and WQBO years, we examine the Rossby wave source (RWS) in EQBO and WQBO years, separately. In MJO phase 2, negative RWS covers a large area from Central to East Asia and positive RWS appears over the Arabian Peninsula in EQBO years (Fig. 6a). The positive and negative RWS pattern is associated with the development of wave train over Eurasia (Fig. 4a). The positive and negative RWS are mainly contributed by $-\zeta \nabla \cdot \mathbf{V}'_{\chi}$, which is the stretching of mean absolute vorticity by anomalous divergent winds. Note that ζ is positive, which is determined by the sign of the Coriolis parameter. This result is consistent with Henderson et al.

(2017). In WQBO years, the RWS is weak over Eurasia (Fig. 6b), which corresponds to the weak wave pattern in this case (Fig. 4b).

In MJO phase 3, the RWS pattern over Eurasia weakens in EQBO years (Fig. 6c), which is associated with the weakened wave train in situ (Fig. 4c). In WQBO years, positive–negative–positive RWS extends from eastern Europe towards Central Asia (Fig. 6d). This RWS distribution corresponds to the wave train pattern over Eurasia (Fig. 4d). Comparison of different terms in the RWS equation indicates that the total RWS is largely contributed by the vortex stretching by divergent wind anomalies ($-\zeta \nabla \cdot \mathbf{V}'_{\chi}$) as well.

To reveal the development of the RWS, we present in Fig. 7 anomalous divergent winds in MJO phases 2–3 in both EQBO and WQBO years. In MJO phase 2, anomalous upper-level divergence is observed over the tropical Indian Ocean (Fig. 7a, b). The anomalous divergence is stronger and extends more northward in EQBO years than in WQBO years. It suggests that the MJO convection is stronger in EQBO years, consistent with previous studies (Yoo and Son 2016; Son et al. 2017; Nishimoto and Yoden 2017; Hendon and Abhik 2018; Zhang and Zhang 2018; Andrews et al.

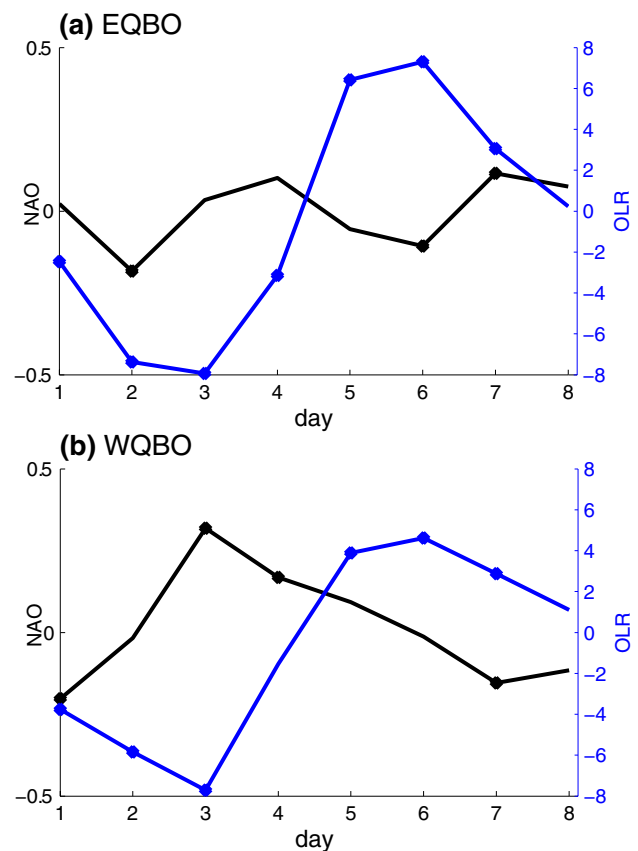


Fig. 5 Time evolution of composite NAO index (black curve), regional mean OLR anomalies (blue curve, W/m^2) over the region 20°S – 20°N , 60°E – 100°E in EQBO (a) and WQBO (b) years. Dots on the curves indicates anomalies significant at the 95% confidence level

2019). Divergence of the upper-level divergent wind anomalies extends from South Asia to East Asia (Fig. 7a), leading to negative $-\bar{\zeta}\nabla \cdot \overline{V}'_{\chi}$ and total RWS there (Fig. 6a). Part of the anomalous upper-level divergent winds converge over the northern Arabian Peninsula (Fig. 7a), leading to positive $-\bar{\zeta}\nabla \cdot \overline{V}'_{\chi}$ and total RWS there (Fig. 6a). The weaker divergent wind anomalies in WQBO years over Eurasia (Fig. 7b) are followed by weaker RWS (Fig. 6b) and thus the wave pattern over Eurasia (Fig. 4b).

In MJO phase 3, the upper-level divergent wind anomalies move eastward (Fig. 7c, d). The divergent wind anomalies are weaker than those in MJO phase 2 in EQBO years (Fig. 7c), which corresponds to the weak RWS and wave pattern over Eurasia (Figs. 4c, 6c). In WQBO years, anomalous divergent winds become stronger than those in MJO phase 2 (Fig. 7d). Convergence of anomalous divergent winds can be found over eastern Europe and Central Asia, which leads to positive $-\bar{\zeta}\nabla \cdot \overline{V}'_{\chi}$ and total RWS (Fig. 6d). The divergence of anomalous divergent winds appears west of the Caspian Sea (Fig. 7d), leading to negative $-\bar{\zeta}\nabla \cdot \overline{V}'_{\chi}$ and total RWS (Fig. 6d).

Previous studies have indicated that the MJO convection can induce anomalous ascending motion and thus trigger anomalous meridional overturning circulation that modulates the mid-latitude circulation (He et al. 2011; Seo et al. 2017). The development and southward intrusion of the Siberian high that leads to cold anomalies over East Asia can be linked to the MJO phases 2–3 via an anomalous meridional circulation (Song and Wu 2019c). The analysis in the previous section shows that the surface anticyclonic anomalies associated with cold anomalies over Eurasia are different in EQBO and WQBO years (Fig. 2). This difference appears to be related to discrepancies in the MJO-related meridional overturning circulation in EQBO and WQBO years. This is illustrated using Fig. 8 that depicts a latitude–height cross section along 80° E–100° E in MJO phases 2–3 for EQBO and WQBO years.

In MJO phase 2, an anomalous overturning circulation is evident between the tropics-subtropics and mid-latitude extending from 15° N to 60° N in EQBO years (Fig. 8a). Upper-level anomalous poleward divergent winds and lower-level anomalous equatorward divergent winds connect

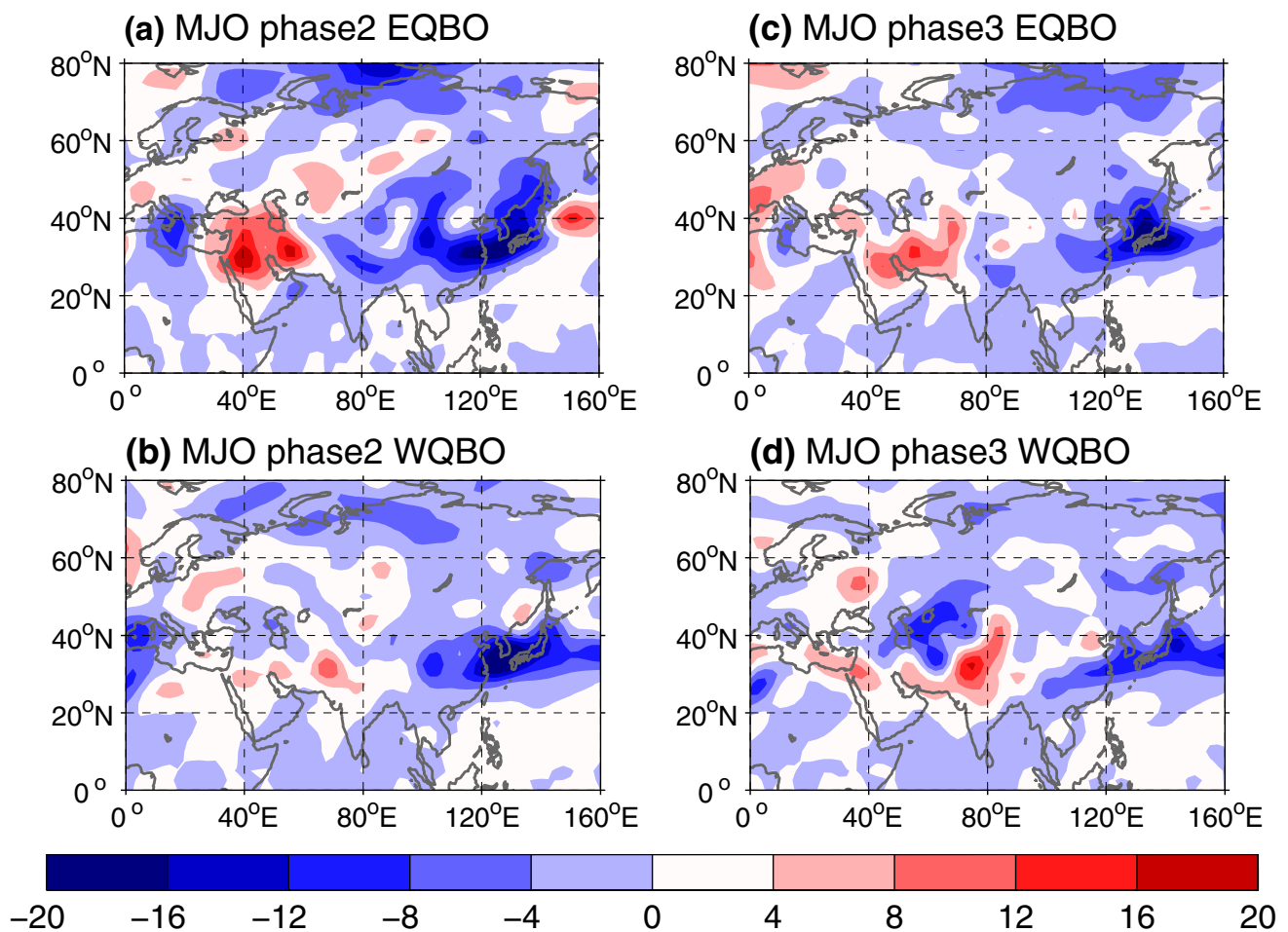


Fig. 6 Anomalous Rossby wave source at 200 hPa (RWS, shading, $\times 10^{-11}/s^2$) in MJO phases 2 (a, b) and 3 (c, d) in EQBO (a, c) and WQBO (b, d) years

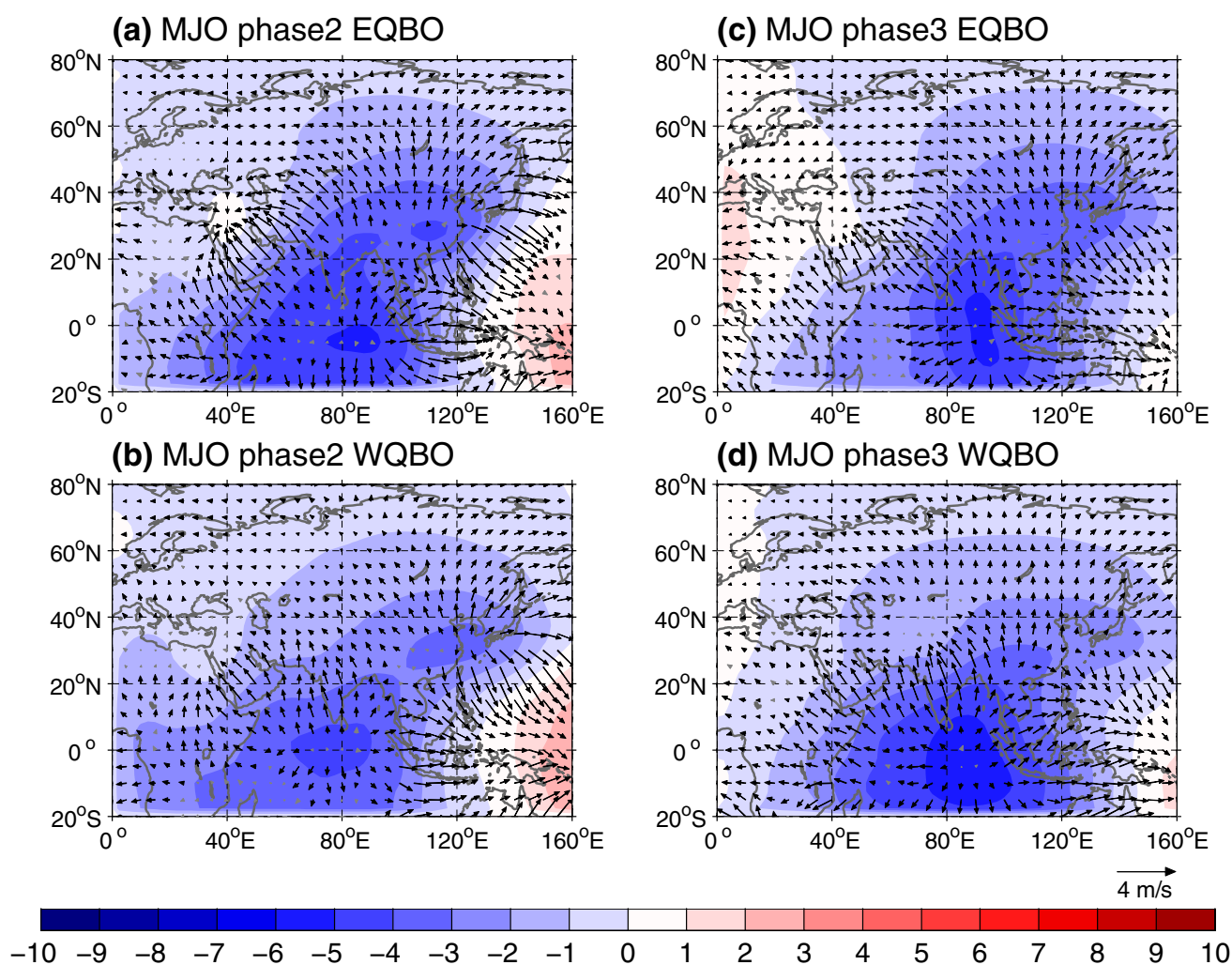


Fig. 7 Composite anomalies of velocity potential at 200 hPa (shading, $\times 10^6/s$) and the corresponding divergent winds (vector, m/s, scale at the right-bottom) in MJO phases 2 (**a**, **b**) and 3 (**c**, **d**) in

EQBO (**a**, **c**) and WQBO (**b**, **d**) years. Black vectors denote divergent wind anomalies significant at the 95% confidence level

anomalous ascending motion around 15° N and anomalous descending motion around 60° N. This suggests that the MJO convection in EQBO years can induce anomalous vertical circulation and descending motion over the mid-latitude, which leads to the development of surface anticyclonic anomalies (Fig. 2a). In WQBO years, both the tropical anomalous ascending and mid-latitude anomalous descending motion are weaker (Fig. 8b), indicative of a weak connection between tropical MJO convection and the mid-latitude. This corresponds to weaker surface anticyclonic anomalies over western Siberia (Fig. 2b). This is related to weaker MJO convection in MJO phase 2 in WQBO years than in EQBO years.

In MJO phase 3, the anomalous meridional overturning circulation between the tropics and mid-latitude still exists in EQBO years, but the anomalous descending motion

displaces southward compared to MJO phase 2 (Figs. 8c). In WQBO years, the MJO-related overturning circulation is apparent from the tropics toward mid-latitude, but the northward reach of the anomalous descending is limited to south of 40° N (Fig. 8d). This corresponds to a limited northward extension of poleward divergent wind anomalies (Fig. 7d).

5 Summary and discussions

Previous studies have indicated that the MJO can induce intraseasonal surface air temperature anomalies over Eurasia. The MJO can be modified by the QBO in the stratosphere during boreal winter. The activities of the MJO have been found to be stronger and last longer in EQBO years than WQBO years. In this study, we found that the MJO induced intraseasonal surface air temperature anomalies

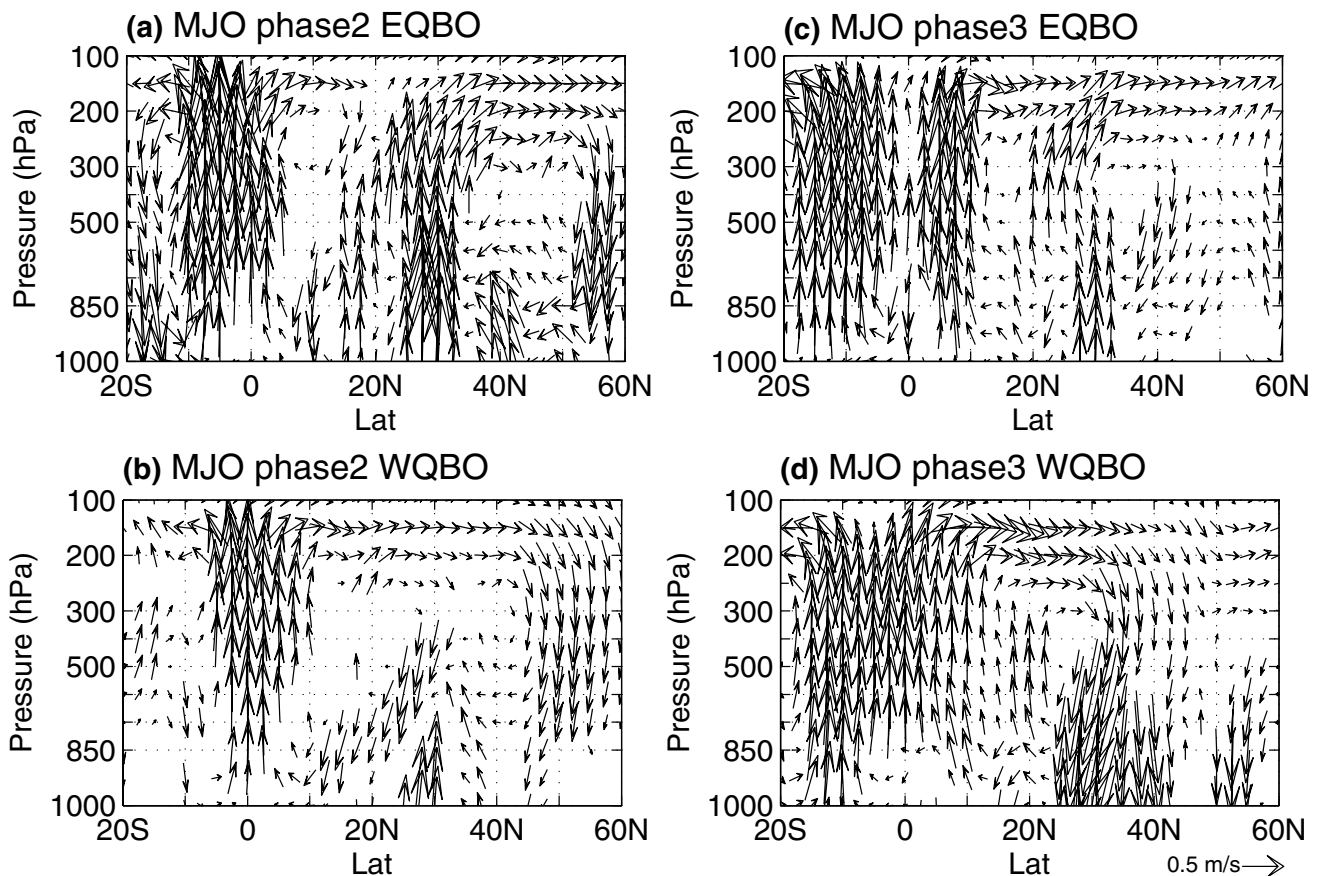


Fig. 8 Composite anomalies of vertical circulation consisting of divergent meridional wind (m/s) and vertical p -velocity (0.01 Pa/s) along 80° E– 100° E in MJO phases 2 (**a**, **b**) and 3 (**c**, **d**) in EQBO

(**a**, **c**) and WQBO (**b**, **d**) years. Only anomalies significant at the 95% confidence level are plotted

over Eurasia are different in the QBO easterly and westerly phases. This difference is associated with the effects of MJO and NAO on the mid-latitude wave train and anomalous surface anticyclone/cyclone over Eurasia, which is summarized in Fig. 9.

In EQBO years, intraseasonal surface air temperature anomalies associated with the MJO phase 2 are manifested as a meridional dipole pattern over Eurasia. It is related to the development of mid-latitude surface anticyclonic anomalies (Fig. 9a), which is linked to the combined effect of the mid-latitude wave train associated with the negative NAO and poleward propagation of Rossby wave train triggered by the stronger MJO convection in EQBO years. The negative NAO is related to the EQBO through the Holton–Tan relationship. The MJO convection can also induce anomalous local overturning circulation, leading to the development and eastward extension of mid-latitude anticyclonic anomalies. The temperature anomalies over Eurasia are mainly contributed by horizontal advection due to the wind anomalies associated with the surface anticyclonic anomalies.

In WQBO years, the MJO-related intraseasonal surface air temperature anomalies manifest as a zonally extended pattern from Europe to Central Asia, which is related to the development of mid-latitude Rossby wave train associated with the positive NAO (Fig. 9b). The positive NAO in MJO phase 3 is associated with the stronger MJO-NAO connection in WQBO years, which is due to the stronger subtropical jet stream over the North Pacific. As indicated by the model study of Lin and Brunet (2018), the extratropical response of the MJO is nonlinear. The enhancement of the subtropical jet over the North Pacific lead to the intensification of the extratropical response to the MJO (i.e., the PNA-like teleconnection pattern), which favors the Rossby wave propagation (Feng and Lin 2019) that connects the MJO and the NAO. The temperature anomalies over Eurasia are located more westward compared to EQBO years. The upper-level divergent wind anomalies associated with the MJO convection partially contribute to the RWS that leads to the development of mid-latitude wave train. Like the EQBO years, the MJO-related surface temperature anomalies are also associated with horizontal advection during WQBO years, which is

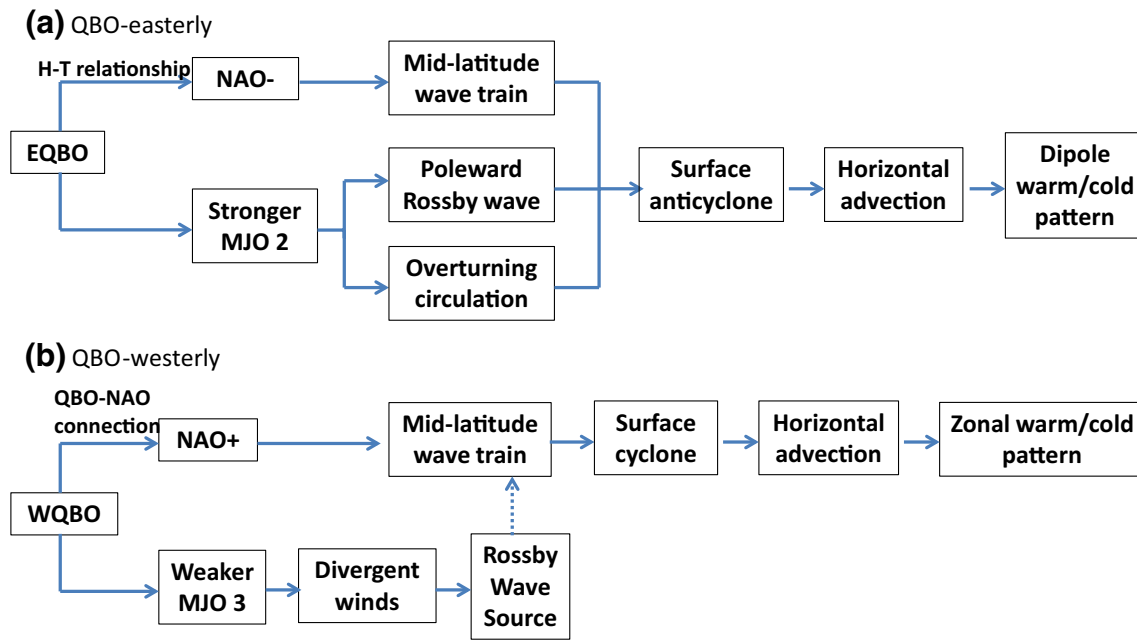


Fig. 9 Mechanistic pathway leading to intraseasonal surface air temperature anomalies over Eurasia in MJO phases 2–3 in EQBO (a) and WQBO (b) years

contributed by the development of surface pressure anomalies and accompanying anomalous winds.

In this study, we found that the modulation of the QBO on the connection between the MJO and NAO can influence surface temperature anomalies over Eurasia. It may be possible that the MJO–AO connection can also be influenced by the QBO phases. Further studies are needed to understand the modulation of QBO on the MJO–AO connection.

The present study focuses on the modulation of QBO on the impact of MJO on intraseasonal surface air temperature anomalies over Eurasia. Since the QBO can modulate the MJO-related teleconnection over the Pacific (Son et al. 2017; Wang et al. 2018), the MJO-related climate over North America may be influenced by the QBO phase. Studies are needed to understand how the QBO affects the influence of the MJO on climate over North America. In this study, we use the reanalysis data to investigate the modulation of the QBO on the MJO-related surface temperature anomalies. In the future, longer time period model data may be used to confirm the results in this study.

Acknowledgments We appreciate comments from two anonymous reviewers that have helped the improvement of this manuscript. This study is supported by the National Natural Science Foundation of China grants (41705063, 41530425, 41721004, and 41475081). The NCEP reanalysis 2 data were obtained from <ftp://ftp.cdc.noaa.gov/>.

References

- Abdillah MR, Kanno Y, Iwasaki T (2018) Tropical–extratropical interactions associated with East Asian cold air outbreaks. Part II: intraseasonal variation. *J Clim* 31:473–490
- Andrews MB, Knight JR, Scaife AA, Lu Y, Wu T, Gray LJ, Schenzinger V (2019) Observed and simulated teleconnections between the stratospheric quasi-biennial oscillation and Northern Hemisphere winter atmospheric circulation. *J Geophys Res Atmos* 124:1219–1232
- Baldwin MP et al (2001) The quasi-biennial oscillation. *Rev Geophys* 39:179–229
- Cassou C (2008) Intraseasonal interaction between the Madden–Julian oscillation and the North Atlantic oscillation. *Nature* 455(7212):523–527
- Flatau M, Kim YJ (2013) Interaction between the MJO and polar circulations. *J Clim* 26:3562–3574
- Feng P-N, Lin H (2019) Modulation of the MJO-related teleconnections by the QBO. *J Geophys Res Atmos* 124(22):12022–12033
- Garfinkel CI, Hartmann DL (2011) The influence of the quasi-biennial oscillation on the troposphere in winter in a hierarchy of models. Part I: simplified dry GCMs. *J Atmos Sci* 68:1273–1289
- Gray LJ, Anstey JA, Kawatani Y, Lu H, Osprey S, Schenzinger V (2018) Surface impacts of the quasi biennial oscillation. *Atmos Chem Phys* 18:8227–8247
- He J, Lin H, Wu Z (2011) Another look at influences of the Madden–Julian oscillation on the wintertime East Asian weather. *J Geophys Res Atmos* 116:D03109
- Hegyi BM, Deng Y (2017) Dynamical and thermodynamical impacts of high- and low-frequency atmospheric eddies on the initial melt of Arctic sea ice. *J Clim* 30:865–883
- Henderson SA, Maloney ED, Son S-W (2017) Madden–Julian oscillation Pacific teleconnections: the impact of the basic state and MJO representation in general circulation models. *J Clim* 30:4567–4587

- Hendon HH, Abhik S (2018) Differences in vertical structure of the Madden–Julian oscillation associated with the quasi-biennial oscillation. *Geophys Res Lett* 45:4419–4428
- Holton JR (2004) An introduction to dynamic meteorology. Elsevier, London, pp 1–535
- Holton JR, Tan H-C (1980) The influence of the equatorial quasi-biennial oscillation on the global circulation at 50 mb. *J Atmos Sci* 37:2200–2208
- Holton JR, Tan H-C (1982) The quasi-biennial oscillation in the Northern Hemisphere lower stratosphere. *J Meteorol Soc Jpn Ser II* 60:140–148
- Jeong J-H, Ho C-H (2005) Changes in occurrence of cold surges over East Asia in association with Arctic oscillation. *Geophys Res Lett* 32:L14704
- Jin F, Hoskins BJ (1995) The direct response to tropical heating in a baroclinic atmosphere. *J Atmos Sci* 52:307–319
- Kanamitsu M, Ebisuzaki W, Woollen J, Yang S-K, Hnilo JJ, Fiorino M, Potter GL (2002) NCEP–DOE AMIP-II reanalysis (R-2). *Bull Am Meteorol Soc* 83:1631–1643
- L’Heureux ML, Higgins RW (2008) Boreal winter links between the Madden–Julian oscillation and the Arctic oscillation. *J Clim* 21:3040–3050
- Li X, Gollan G, Greatbatch RJ, Lu R (2018) Intraseasonal variation of the East Asian summer monsoon associated with the Madden–Julian oscillation. *Atmos Sci Lett* 19:e794
- Lin H, Brunet G (2018) Extratropical response to the MJO: nonlinearity and sensitivity to the initial state. *J Atmos Sci* 75(1):219–234
- Lin H, Brunet G, Derome J (2009) An observed connection between the North Atlantic oscillation and the Madden–Julian oscillation. *J Clim*
- Liu C, Tian B, Li KF, Manney GL, Livesey NJ, Yung YL, Waliser DE (2014) Northern Hemisphere mid-winter vortex-displacement and vortex-split stratospheric sudden warmings: influence of the Madden–Julian oscillation and quasi-biennial oscillation. *J Geophys Res Atmos* 119:12599–12620
- Madden RA, Julian PR (1971) Detection of a 40–50 day oscillation in the zonal wind in the tropical Pacific. *J Atmos Sci* 28:702–708
- Madden RA, Julian PR (1972) Description of global-scale circulation cells in the tropics with a 40–50 day period. *J Atmos Sci* 29:1109–1123
- Nishimoto E, Yoden S (2017) Influence of the stratospheric quasi-biennial oscillation on the Madden–Julian oscillation during austral summer. *J Atmos Sci* 74:1105–1125
- Peña-Ortiz C, Manzini E, Giorgetta MA (2019) Tropical deep convection impact on southern winter stationary waves and its modulation by the quasi-biennial oscillation. *J Clim* 32:7453–7467
- Rao J, Ren R-C (2016) A decomposition of ENSO’s impacts on the northern winter stratosphere: competing effect of SST forcing in the tropical Indian Ocean. *Clim Dyn* 46:3689–3707
- Rao J, Ren R-C (2017) Parallel comparison of the 1982/83, 1997/98, and 2015/16 super El Niños and their effects on the extratropical stratosphere. *Adv Atmos Sci* 34:1121–1133
- Rao J, Ren R-C (2018) Varying stratospheric responses to tropical Atlantic SST forcing from early to late winter. *Clim Dyn* 51(5–6):2079–2096
- Rao J, Yu Y, Guo D, Shi C, Chen D, Hu D (2019) Evaluating the Brewer–Dobson circulation and its responses to ENSO, QBO, and the solar cycle in different reanalyses. *Earth Planet Phys* 3(2):166–181
- Sardeshmukh PD, Hoskins BJ (1988) The generation of global rotational flow by steady idealized tropical divergence. *J Atmos Sci* 45:1228–1251
- Seo K-H, Lee H-J (2017) Mechanisms for a PNA-like teleconnection pattern in response to the MJO. *J Atmos Sci* 74:1767–1781
- Son S-W, Lim Y, Yoo C, Hendon HH, Kim J (2017) Stratospheric control of the Madden–Julian oscillation. *J Clim* 30:1909–1922
- Song L, Wu R (2017) Processes for occurrence of strong cold events over eastern China. *J Clim* 30:9247–9266
- Song L, Wu R (2019a) Combined effects of the MJO and the Arctic oscillation on the intraseasonal eastern China winter temperature variations. *J Clim* 32:2295–2311
- Song L, Wu R (2019b) Different cooperation of the Arctic oscillation and the Madden–Julian oscillation in the East Asian cold events during early and late winter. *J Geophys Res Atmos* 124:4913–4931
- Song L, Wu R (2019c) Impacts of MJO convection over the maritime continent on eastern China cold temperatures. *J Clim* 32:3429–3449
- Song L, Wang L, Chen W, Zhang Y (2016) Intraseasonal variation of the strength of the East Asian trough and its climatic impacts in boreal winter. *J Clim* 29:2557–2577
- Takaya K, Nakamura H (2001) A formulation of a phase-independent wave-activity flux for stationary and migratory quasigeostrophic eddies on a zonally varying basic flow. *J Atmos Sci* 58:608–627
- Tseng K-C, Maloney E, Barnes E (2019) The consistency of MJO teleconnection patterns: an explanation using linear Rossby wave theory. *J Clim* 32:531–548
- Wang J, Kim H-M, Chang EKM (2018) Interannual modulation of Northern Hemisphere winter storm tracks by the QBO. *Geophys Res Lett* 45:2786–2794
- Watanabe M (2004) Asian jet waveguide and a downstream extension of the North Atlantic oscillation. *J Clim* 17:4674–4691
- Wheeler MC, Hendon HH (2004) An all-season real-time multivariate MJO index: development of an index for monitoring and prediction. *Mon Weather Rev* 132:1917–1932
- Yoo C, Son S-W (2016) Modulation of the boreal wintertime Madden–Julian oscillation by the stratospheric quasi-biennial oscillation. *Geophys Res Lett* 43:1392–1398
- Zhang C (2005) Madden–Julian oscillation. *Rev Geophys* 43:RG2003
- Zhang C, Zhang B (2018) QBO–MJO connection. *J Geophys Res Atmos* 123:2957–2967
- Zhou S, Miller AJ (2005) The interaction of the Madden–Julian oscillation and the Arctic oscillation. *J Clim* 18:143–159

Publisher’s Note Springer Nature remains neutral with regard to jurisdictional claims in published maps and institutional affiliations.